

Clutter Rejecting Waveforms for Synthetic Aperture Radar Traversing Arbitrary Flight Path

Birsen Yazici
Department of Electrical, Computer
& Systems Engineering
Rensselaer Polytechnic Institute
Troy, NY 12180
Email: yazici@ecse.rpi.edu

Can Evren Yarman
Department of Electrical, Computer
& Systems Engineering
Rensselaer Polytechnic Institute
Troy, NY 12180
Email: yarman@rpi.edu

Margaret Cheney
Department of Mathematical Sciences
Rensselaer Polytechnic Institute
Troy, NY 12180
Email: cheney@rpi.edu

Abstract—In [28], we presented a synthetic aperture radar (SAR) inversion method in which the backscatter measurements are collected from known but arbitrary flight path and non-flat topography corrupted with clutter and noise. The objective of the current work is to design transmit waveforms and receive filters jointly to perform clutter suppression by adaptive transmit. Our approach starts with the development of a physics based forward model for SAR. Next, we formulate design of clutter rejecting waveforms as a variational problem using the minimum mean square error criteria. The resulting waveforms lead to an adaptive linear least squares transmit scheme in which waveforms vary at every point on the flight path based on the clutter and target spectral density functions.

I. INTRODUCTION

In Synthetic Aperture Radar (SAR) imaging [6], [8], [10], [12], [22], [27], a plane or satellite carrying an antenna moves along a flight path. The antenna emits pulses of electromagnetic radiation, which scatter off the terrain, and the scattered waves are measured with the same antenna. The received signals are then used to produce an image of the terrain.

The nature of the imaging problem depends on the directivity of the antenna. We are interested particularly in the case of antennas with poor directivity, where the antenna footprint is large and standard narrow-beam imaging methods are not useful. This is typically the case for foliage-penetrating radar [26], [27], whose low frequencies do not allow for much beam focusing.

There are two main classes of imaging algorithms, one statistical and the other deterministic. Both approaches encompass many specialized techniques, however, deterministic approaches do not have an explicit mechanism to incorporate statistical information about the scene, noise, or clutter.

Some attempts have been made to develop edge-preserving reconstruction algorithms for SAR [4], [5]. These approaches are typically very computationally intensive. In this paper, we show how statistical information can be incorporated into a class of deterministic imaging algorithms relevant for radar imaging. Our approach has the advantage of providing an

algorithm whose computational burden is less severe than that of some other approaches.

The methods we use in this paper are based on microlocal analysis [9], [13], [25], which is a theory for dealing with oscillatory integrals and singularities. These microlocal methods enable us to reconstruct edges and boundaries between different materials in the scattering region [2], [1], [3], [17], [20], [21]. These edges and boundaries correspond mathematically to singularities in the reflectivity function; an image of these singularities gives us an image of structures such as walls and vehicles. The microlocal approach has the advantage of providing reconstruction formulas even in the case when the data are incomplete and non-ideal. In addition, these methods can accommodate the varying antenna beam patterns that arise in the cases of non-ideal antenna motion and gain, and with appropriate adjustments the same reconstruction formulas apply to both spotlight-mode [7] and stripmap-mode radar [10], [12]. Microlocal reconstruction techniques have been used to advantage in the geophysics community, where the resulting algorithms have been found to be fast and robust [2], [3].

Microlocal methods have the limitation that they can only be expected to provide a reconstruction of singularities and their strengths. However, in practice they often reduce to the exact inversion formulas that are known for idealized cases. This is the case here: our reconstruction formula reduces to the exact inversion formula of [11], [14], [18] for the case of a perfect point source moving along a single straight flight track above a flat earth. Furthermore, when there is no noise and clutter; and no statistical information on the target is available, our inversion formula reduces to the deterministic one presented in [19].

The microlocal approach leads to generalized *filtered backprojection* algorithms for image reconstruction. In this paper, we show how the filter can be designed to incorporate statistical information about the target, noise and clutter into the transmitted waveform.

The paper is organized as follows. Section II introduces

the mathematical model and relevant notation. Section III develops the image formation algorithm, explains how the transmitted waveform and the filter should be chosen in the image formation and generalized filtered backprojection algorithm. Section IV presents numerical simulations. Finally, Section V summarizes our results and conclusion.

II. THE MATHEMATICAL MODEL

We model the antenna as a time-varying current density $\tilde{j}(t, \mathbf{x})$ over an aperture. This is appropriate for a wide variety of antennas. For the rest of the paper, we will focus to the model $\tilde{j}(t, \mathbf{x}) = p(t)j_{tr}(\mathbf{x})$, where $p(t)$ is the transmitted waveform, referred to as the pulse, and $j_{tr}(\mathbf{x})$ is the waveguide. For this case, the field emanating from the antenna satisfies the scalar wave equation

$$(\nabla^2 - c_0^{-2}\partial_t^2)u^{in}(t, \mathbf{x}) = -p(t)j_{tr}(\mathbf{x}), \quad (1)$$

where c_0 is the speed of light in dry air.

From (1), we use the Green's function [24] to obtain

$$u^{in}(t, \mathbf{x}) = g_0 * (pj_{tr}) = \int \frac{e^{-i\omega(t-|\mathbf{x}-\mathbf{y}|/c_0)}}{4\pi|\mathbf{x}-\mathbf{y}|} P(\omega)j_{tr}(\mathbf{y})d\omega d\mathbf{y}, \quad (2)$$

where $P(\omega) = \frac{1}{2\pi} \int p(t)e^{it\omega}dt$. Next we assume that the antenna (or sensor array) is small compared with the distance to the scatterers. In the far field, we can express the incident field

$$u^{in}(t, \mathbf{x}, \mathbf{y}) \approx \int \frac{e^{-i\omega(t-|\mathbf{x}-\mathbf{y}|/c_0)}}{4\pi|\mathbf{x}-\mathbf{y}|} P(\omega)J_{tr}(\omega/c_0(\widehat{\mathbf{x}-\mathbf{y}}), \mathbf{y})d\omega, \quad (3)$$

where $\widehat{\mathbf{x}-\mathbf{y}}$ denotes a unit vector in the same direction as $\mathbf{x}-\mathbf{y}$, \mathbf{y} now denotes the center of the antenna and

$$J_{tr}(\omega/c_0(\widehat{\mathbf{x}-\mathbf{y}}), \mathbf{y}) = e^{i\omega/c_0(\widehat{\mathbf{x}-\mathbf{y}})\cdot\mathbf{y}} \int e^{-i\omega/c_0(\widehat{\mathbf{x}-\mathbf{y}})\cdot\mathbf{v}} j_{tr}(\mathbf{v})d\mathbf{v}. \quad (4)$$

A. A model for the scattering field

The model we use for wave propagation, including the source, is

$$(\nabla^2 - c^{-2}(\mathbf{x})\partial_t^2)u(t, \mathbf{x}) = -p(t)j_{tr}(\mathbf{x}). \quad (5)$$

where $c(\mathbf{x})$ is the speed of light in the medium. We write $u = u^{in} + u^{sc}$ in (5) and use (1) to obtain

$$(\nabla^2 - c_0^{-2}\partial_t^2)u^{sc}(t, \mathbf{x}) = V(\mathbf{x})\partial_t^2 u(t, \mathbf{x}), \quad (6)$$

where

$$V(\mathbf{x}) = \frac{1}{c^2(\mathbf{x})} - \frac{1}{c_0^2}. \quad (7)$$

The *reflectivity function* V contains all the information about how the scattering medium differs from free space. It is V , or at least its discontinuities and other singularities, that we want to recover.

The *Born or single-scattering approximation* [15], [16] to the scattered field u^{sc} is obtained by replacing the full field u

on the right side of (1) by the incident field u^{in} . Solving the resulting differential equation leads to

$$\begin{aligned} u^{sc}(t, \mathbf{x}) &\approx - \int g_0(t-\tau, \mathbf{x}-\mathbf{z})V(\mathbf{z})\partial_\tau^2 u^{in}(\tau, \mathbf{z})d\tau d\mathbf{z} \\ &= - \int \frac{V(\mathbf{z})}{4\pi|\mathbf{x}-\mathbf{z}|} \partial_t^2 u^{in}(t, \mathbf{z})d\mathbf{z}. \end{aligned} \quad (8)$$

For the incident field (3), (8) becomes

$$\begin{aligned} u^{sc}(t, \mathbf{x}, \mathbf{y}) &\approx \int \frac{e^{-i\omega(t-(|\mathbf{x}-\mathbf{z}|+|\mathbf{z}-\mathbf{y}|)/c_0)}}{(4\pi)^2|\mathbf{x}-\mathbf{z}||\mathbf{z}-\mathbf{y}|} \\ &\quad \times \omega^2 P(\omega)J_{tr}(\omega/c_0(\widehat{\mathbf{z}-\mathbf{y}}), \mathbf{y})V(\mathbf{z})d\omega d\mathbf{z}. \end{aligned} \quad (9)$$

B. A model for the ideal received signal

The field is measured by the receiving antenna; the reception process results in a beam pattern for reception $J_{rc}(\omega/c_0(\widehat{\mathbf{z}-\mathbf{x}}), \mathbf{x})$. Thus a model for the signal received at \mathbf{x} from a source at \mathbf{y} is

$$\begin{aligned} u^{sc}(t, \mathbf{x}, \mathbf{y}) &\approx \int \frac{e^{-i\omega(t-(|\mathbf{x}-\mathbf{z}|+|\mathbf{z}-\mathbf{y}|)/c_0)}}{(4\pi)^2|\mathbf{x}-\mathbf{z}||\mathbf{z}-\mathbf{y}|} \omega^2 P(\omega) \\ &\quad \times J_{rc}(\omega/c_0(\widehat{\mathbf{z}-\mathbf{x}}), \mathbf{x})J_{tr}(\omega/c_0(\widehat{\mathbf{z}-\mathbf{y}}), \mathbf{y})V(\mathbf{z})d\omega d\mathbf{z}. \end{aligned} \quad (10)$$

For monostatic SAR, $J_{rc} = J_{tr}$ and $\mathbf{x} = \mathbf{y}$ since the transmit and receive antenna is the same. Thus, the ideal received signal becomes

$$\tilde{u}^{sc}(t, \mathbf{y}) \approx \int e^{-i\omega(t-2|\mathbf{y}-\mathbf{z}|/c_0)} W(\mathbf{x}, \mathbf{y}, \omega)V(\mathbf{z})d\omega d\mathbf{z}, \quad (11)$$

where

$$W(\mathbf{x}, \mathbf{y}, \omega) = \frac{\omega^2 P(\omega)J_{tr}^2(\omega/c_0(\widehat{\mathbf{z}-\mathbf{y}}), \mathbf{y})}{(4\pi)^2|\mathbf{y}-\mathbf{z}|^2}. \quad (12)$$

We assume the earth's surface is located at the position given by $\mathbf{z} = \psi(\mathbf{x})$, where $\psi: \mathbb{R}^2 \rightarrow \mathbb{R}^3$ is known. Because electromagnetic waves are rapidly attenuated in the earth, we assume that the scattering takes place in a thin region near the surface; thus we assume that the perturbation in wave speed c is of the form $c^{-2}(\mathbf{z}) - c_0^{-2} = V(\mathbf{z})\delta(\mathbf{z} - \psi(\mathbf{x}))$. Here c_0 is the speed of light in dry air, and V , the *ground reflectivity function*, is the quantity we wish to image. Then the received field at sensor location \mathbf{y} and time t can be approximated by the expression [19]

$$\tilde{u}^{sc}(\mathbf{y}, t) = \iint e^{-i\omega(t-2|\psi(\mathbf{x})-\mathbf{y}|/c_0)} W(\mathbf{x}, \mathbf{y}, \omega)V(\mathbf{x})d\omega d^2\mathbf{x}, \quad (13)$$

where ω denotes the angular frequency. Because this waveform is bandlimited, ultimately we reconstruct band-limited approximations to singularities rather than the actual singularities.

We modify the model (13) in two ways. First, we assume that V is composed of two pieces: $V = \rho_T + \rho_C$, where ρ_T corresponds to a target in which we are interested, and ρ_C corresponds to other scatterers in which we are not interested, referred to as clutter. Second, we include additive noise n , which models thermal fluctuations in the receiver.

The idealized inverse problem is to determine ρ_T from knowledge of $\tilde{u}^{sc} + n$ for $t \in (T_1, T_2)$ and for \mathbf{y} on a curve. We parameterize this curve by $\gamma := \{ \gamma(s) : s_{\min} < s < s_{\max} \}$. We will write $\mathbf{R}_{s,\mathbf{x}} = \psi(\mathbf{x}) - \gamma(s)$.

The data is $d = \tilde{u}^{sc} + n$:

$$d(t, s) = F[V](t, s) + n(t, s), \quad (14)$$

where

$$F[V](t, s) = \int e^{-i\omega[t-2|\mathbf{R}_{s,\mathbf{x}}|/c]} A(\mathbf{x}, s, \omega) V(\mathbf{x}) d^2\mathbf{x}. \quad (15)$$

Here $A(\mathbf{x}, s, \omega) = W(\mathbf{x}, \gamma(s), \omega)$ is given by

$$A(\mathbf{x}, s, \omega) = \frac{\omega^2 P(\omega) J_{tr}^2(w/c_o(\widehat{R}_{s,\mathbf{x}}), \gamma(s))}{(4\pi)^2 |\widehat{R}_{s,\mathbf{x}}|^2}. \quad (16)$$

and $n(t, s)$ denotes the receiver noise.

We make the following assumptions about the statistics. First, we assume that the noise is stationary in the fast time component t and statistically uncorrelated in the slow time component s , so that

$$\int e^{-i\omega t} e^{-i\omega' t'} E[n(t, s)n(t', s')] dt dt' = S_N(\omega, s) \delta(\omega + \omega') \delta(s - s'), \quad (17)$$

where E denotes the expected value. Similarly we write

$$E[\rho_T(\mathbf{x})\rho_T(\mathbf{x}')] = \mathcal{R}_T(\mathbf{x}, \mathbf{x}') \quad (18)$$

$$E[\rho_C(\mathbf{x})\rho_C(\mathbf{x}')] = \mathcal{R}_C(\mathbf{x}, \mathbf{x}'), \quad (19)$$

where we assume

$$\mathcal{R}_T(\mathbf{x}, \mathbf{x}') = \iint e^{-i\mathbf{x}\cdot\boldsymbol{\eta}} e^{i\mathbf{x}'\cdot\boldsymbol{\eta}'} \tilde{S}_T(\boldsymbol{\eta}, \boldsymbol{\eta}') d\boldsymbol{\eta} d\boldsymbol{\eta}' \quad (20)$$

$$\mathcal{R}_C(\mathbf{x}, \mathbf{x}') = \iint e^{-i\mathbf{x}\cdot\boldsymbol{\eta}} e^{i\mathbf{x}'\cdot\boldsymbol{\eta}'} \tilde{S}_C(\boldsymbol{\eta}, \boldsymbol{\eta}') d\boldsymbol{\eta} d\boldsymbol{\eta}'. \quad (21)$$

In addition, we assume that the amplitude A of (15) satisfies

$$\sup_{(s,t,\mathbf{x}) \in K} | \partial_\omega^\alpha \partial_s^\beta \partial_{x_1}^{\rho_1} \partial_{x_2}^{\rho_2} A(\mathbf{x}, s, \omega) | \leq C (1 + \omega^2)^{(2-|\alpha|)/2} \quad (22)$$

where K is any compact subset of $\mathbb{R}_s \times \mathbb{R}_{\mathbf{x}}^2$, and the constant C depends on K, β, δ, ρ_1 , and ρ_2 . This assumption is needed in order to make various stationary phase calculations hold; in fact this assumption makes the ‘‘forward’’ operator F a Fourier Integral Operator [9], [25], [13]. This assumption is valid, for example, when the source waveform p is a short pulse and the antenna is sufficiently broadband. We note that A can be complex; it can thus be used to model non-ideal antenna behavior such as phase aberrations and frequency-dependent changes in the beam pattern.

III. IMAGE FORMATION

We form the image $\tilde{\rho}_T$ by means of a filtered backprojection operator B : we write $\tilde{\rho}_T(\mathbf{z}) := Bd(\mathbf{z})$, where

$$Bd(\mathbf{z}) := \iint Q(\mathbf{z}, s, \omega) e^{i\omega[t-2|\mathbf{R}_{s,\mathbf{z}}|/c]} d(t, s) dt ds, \quad (23)$$

where Q is determined below.

In [28], to determine Q , we examined the degree to which the image $\tilde{\rho}_T$ reproduces the true ρ_T , or at least the best approximation to ρ_T we could hope to obtain from our limited data. The best approximation to ρ_T was determined by the flight path and the frequency band of the radar system. In particular, the best mean-square approximation ρ_Ω to ρ_T is

$$\begin{aligned} \rho_\Omega(\mathbf{z}) &= I_\Omega \rho_T(\mathbf{z}) = \frac{1}{(2\pi)^2} \int_{\Omega_z} e^{i(\mathbf{z}-\mathbf{x})\cdot\boldsymbol{\xi}} \rho_T(\mathbf{x}) d^2\mathbf{x} \\ &= \frac{1}{(2\pi)^2} \int e^{i(\mathbf{z}-\mathbf{x})\cdot\boldsymbol{\xi}} \chi_{\Omega_z}(\mathbf{x}) \rho_T(\mathbf{x}) d^2\mathbf{x}, \end{aligned} \quad (24)$$

where Ω_z denotes the set of $\boldsymbol{\xi}$ determined by the flight path and frequency band and where χ_{Ω_z} is the function that is 1 if \mathbf{x} is in the set Ω_z and zero otherwise. In [28] we have shown that this set consists of those $\boldsymbol{\xi}$ obtained from (Stolt) change of variables

$$(s, \omega) \rightarrow \boldsymbol{\xi} = \frac{-2\omega}{c} \widehat{R}_{s,\mathbf{z}} \cdot D\psi(\mathbf{z}). \quad (25)$$

as s varies over $[s_{\min}, s_{\max}]$ and ω varies over the frequency band of the system. Here $D\psi$ denotes the 3×2 Jacobian matrix.

A. Determination of the pulse P and filter Q

We would like to determine the pulse P and filter Q so that $\tilde{\rho}$ obtained from (23) is as close as possible to ρ_Ω . In particular, we want to determine P and Q in order to minimize the quantity

$$\Delta(Q, P) = E \left[\int |B(F[V] + n)(\mathbf{z}) - I_\Omega \rho_T(\mathbf{z})|^2 d^2\mathbf{z} \right], \quad (26)$$

where E denotes expected value. The \mathbf{z} -integral of (26) is simply the L^2 -norm, which can be written as the inner product $\langle \cdot, \cdot \rangle$:

$$\begin{aligned} \Delta(Q, P) &= E \langle (BF - I_\Omega)\rho_T + BF\rho_C + Bn, \\ &\quad (BF - I_\Omega)\rho_T + BF\rho_C + Bn \rangle \\ &= \Delta_T(Q) + \Delta_C(Q) + \Delta_N(Q), \end{aligned} \quad (27)$$

where

$$\Delta_T(Q, P) = E \langle (BF - I_\Omega)\rho_T, (BF - I_\Omega)\rho_T \rangle \quad (28)$$

$$\Delta_C(Q, P) = E \langle BF\rho_C, BF\rho_C \rangle \quad (29)$$

$$\Delta_N(Q, P) = E \langle Bn, Bn \rangle \quad (30)$$

We note that the cross terms of (27) disappear because we are assuming that the statistics of the target, clutter, and noise are all mutually independent.

In [28], under the stationarity assumption

$$\begin{aligned} \tilde{S}_T(\boldsymbol{\xi}, \boldsymbol{\xi}') &= S_T(\boldsymbol{\eta}) \delta(\boldsymbol{\xi} - \boldsymbol{\xi}') \\ \tilde{S}_C(\boldsymbol{\xi}, \boldsymbol{\xi}') &= S_C(\boldsymbol{\eta}) \delta(\boldsymbol{\xi} - \boldsymbol{\xi}'), \end{aligned} \quad (31)$$

(28), (29) and (30) were simplified to

$$\begin{aligned} \Delta_T(Q, P) &= \iint | [Q(\mathbf{z}, \boldsymbol{\xi}) A(\mathbf{z}, \boldsymbol{\xi}) J(\mathbf{z}, \boldsymbol{\xi}) - \chi_{\Omega_z}(\boldsymbol{\xi})]^2 dz d\boldsymbol{\xi} \\ \Delta_C(Q, P) &= \iint | Q(\mathbf{z}, \boldsymbol{\xi}) A(\mathbf{z}, \boldsymbol{\xi}) J(\mathbf{z}, \boldsymbol{\xi}) |^2 dz d\boldsymbol{\xi} \\ \Delta_N(Q, P) &= \iint | Q(\mathbf{z}, \boldsymbol{\xi}) |^2 J(\mathbf{z}, \boldsymbol{\xi}) S_N(\boldsymbol{\xi}) dz d\boldsymbol{\xi}, \end{aligned} \quad (32)$$

where $J(\mathbf{z}, s, \omega) = |\partial(s, \omega)/\partial\xi|$ is the determinant of the Jacobian that comes from the change of variables (25). Substituting (32) in (27), we obtained

$$Q = \frac{\chi_\Omega S_T \bar{A}}{|A|^2 J[S_T + S_C] + S_N}, \quad (33)$$

by calculating the variation of Δ with respect to Q [28].

Similarly, in order to determine P we calculate the variation of Δ with respect to P :

$$0 = \frac{d}{d\epsilon} \Big|_{\epsilon=0} \Delta(Q, P + \epsilon P_\epsilon) \sim 2\text{Re} \iint \overline{Q A_\epsilon J} \\ \times \left(\int e^{iz \cdot (\xi - \xi')} Q' A' J' (\tilde{S}_T + \tilde{S}_C) - \tilde{S}_T \chi' d\xi' \right) d\xi dz. \quad (34)$$

Here we used the shorthand notation $Q' := Q(\mathbf{z}, \xi)$, $A' := A(\mathbf{z}, \xi)$, $\chi' := \chi(\mathbf{z}, \xi)$, $J' := J(\mathbf{z}, \xi)$ and

$$A_\epsilon(\mathbf{x}, s, \omega) = \frac{\omega^2 P_\epsilon(\omega) J_{tr}^2(\omega/c_0(\widehat{R_{s,\mathbf{x}}}), \gamma(s))}{(4\pi)^2 |R_{s,\mathbf{x}}|^2}, \quad (35)$$

where s and ω are understood to refer to $s(\xi)$ and $\omega(\xi)$, respectively.

It follows from the right hand side of (34) to be 0 for all Q_ϵ , we must have

$$\int e^{iz \cdot (\xi - \xi')} Q' A' J' (\tilde{S}_T + \tilde{S}_C) - \tilde{S}_T \chi' d\xi' = 0. \quad (36)$$

Under the stationarity assumption (31), (36) reduces to

$$Q A J S_T - \chi_\Omega S_T + Q A J S_C = 0, \quad (37)$$

which can be solved explicitly for A as

$$A(\mathbf{x}, s, \omega) = \frac{\chi_\Omega(\mathbf{x}, s, \omega) S_T(s, \omega)}{Q(\mathbf{x}, s, \omega) J(\mathbf{x}, s, \omega) [S_T(s, \omega) + S_C(s, \omega)]}. \quad (38)$$

Multiplying (38) by \bar{A} and substituting into (33), we obtain $Q S_n = 0$ and

$$Q(\mathbf{x}, s, \omega) P(\omega) = \frac{\chi_\Omega(\mathbf{x}, s, \omega) (4\pi)^2 |R_{s,\mathbf{x}}|^2}{\omega^2 J_{tr}^2(\omega/c_0(\widehat{R_{s,\mathbf{x}}}), \gamma(s)) J(\mathbf{x}, s, \omega)} \frac{S_T(s, \omega)}{[S_T(s, \omega) + S_C(s, \omega)]}. \quad (39)$$

If we assume that Q is independent of S_T and S_C , and $P(\omega)$ depends on the curve $\gamma(s)$, i.e. $P(\omega) = P(s, \omega)$, then we can factor (39) to obtain P and Q as

$$P(\omega, s) = \frac{S_T(s, \omega)}{[S_T(s, \omega) + S_C(s, \omega)]} \quad (40)$$

$$Q(\mathbf{x}, s, \omega) = \frac{\chi_\Omega(\mathbf{x}, s, \omega) (4\pi)^2 |R_{s,\mathbf{x}}|^2}{\omega^2 J_{tr}^2(\omega/c_0(\widehat{R_{s,\mathbf{x}}}), \gamma(s)) J(\mathbf{x}, s, \omega)}. \quad (41)$$

IV. NUMERICAL SIMULATIONS

We performed numerical simulations to demonstrate the performance of transmitted pulse P and the reconstruction filter Q when chosen as in (40) and (41), respectively.

We make the following assumptions in our numerical simulations. We assume the earth surface is flat. We assume that there are no noise in the measurements, i.e. $S_N = 0$. We assume that $A/P \equiv 1$, hence choose $Q = \chi_\Omega/J$. The region of reconstruction lies within the circle centered at (25km, 25km) with radius 25km where we denote the origin by (0, 0). We normalize all the distances with respect to origin by 10km, i.e. if H denotes the height of the flight path then $H = 1.5$ implies that the height is 15km.

We set the flight trajectory to be a circle centered at (25km, 25km) with radius equal to 30km at 15km above the ground (see Figure 1), i.e.

$$\gamma(s) = (2.5 + 3 \cos s, 2.5 + 3 \sin s, 1.5), \quad s \in [0, 2\pi). \quad (42)$$

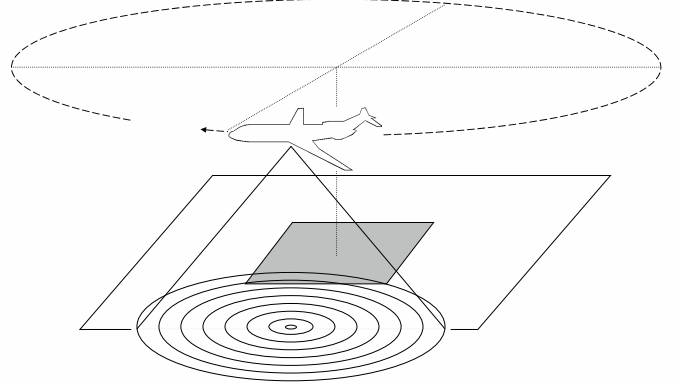


Fig. 1. Acquisition geometry used in the numerical simulations. The flight trajectory is a circle with radius 30km at 15km altitude. The illuminated region is the disc with diameter 50km.

For ease of numerical simulations, and to generate realistic looking targets, we choose analytic functions to represent the target scene T and estimate its power spectral density function by

$$S_T(\zeta) = \left| \int e^{-ix \cdot \zeta} T(\mathbf{x}) d\mathbf{x} \right|^2. \quad (43)$$

Target is then discretized on a grid and its mean and variance are estimated by sample mean and variance estimators. Realization of the clutter process is generated on the discrete grid from Gaussian white noise process using the Karhunen-Loeve transform based on predefined autocovariance or power spectral density functions.

We choose the target scene $T(\mathbf{x})$ as

$$T(x_1, x_2) = \frac{900}{121} \mathbf{1}_{[2,3] \times [2,3]}, \quad (44)$$

where $\chi_{[2,3] \times [2,3]}$ denotes the characteristic function over the square $[2, 3] \times [2, 3]$. The target is discretized on a grid of

51×51 which corresponds to the square region of side 50km with target in its center.

The estimated power spectral density function of the target is

$$S_T(\zeta_1, \zeta_2) = \left(\frac{900 \sin \pi \zeta_1 \sin \pi \zeta_2}{121 \pi^2 \zeta_1 \zeta_2} \right)^2. \quad (45)$$

We choose the power spectral density function of clutter

$$\begin{aligned} S_C(\zeta_1, \zeta_2) &= \frac{1}{4} \sum_{\pm} (S_T(\zeta_1 \pm 8, \zeta_2 \pm 8) + S_T(\zeta_1 \pm 8, \zeta_2 \mp 8)) \\ &= \left(\frac{900}{121} \right)^2 \frac{(\sin \pi \zeta_1)^2 (\sin \pi \zeta_2)^2 (\zeta_2^2 + 64) (\zeta_1^2 + 64)}{\pi^4 (\zeta_1^2 - 64)^2 (\zeta_2^2 - 64)^2}. \end{aligned} \quad (46)$$

We define the signal to clutter ratio (SCR) by

$$SCR = 20 \log \frac{\frac{1}{N} \sum_1^N (T(\mathbf{x}_i) - \mu)^2}{E[\|C\|^2]} \text{dB}, \quad (47)$$

where N is the number of grid points and μ is the mean value of the target scene. Figure 2 shows the target and target embedded in clutter for $SCR = -12\text{dB}$ scenes.

We performed three sets of numerical experiments: reconstruction of i) target in the absence of clutter, i.e. $P \equiv 1$; ii) target embedded in clutter with $SCR = -12\text{dB}$ and $P \equiv 1$; and iii) target embedded in clutter with $SCR = -12\text{dB}$ and P is chosen as in (40). The projection data of the target and the corresponding reconstructed image when $P = 1$ is presented in Figures 3. When the target is embedded in clutter with $SCR = -12\text{dB}$, the projection data and corresponding reconstructed images for $P = 1$ and P chosen as in (40) are presented in Figures 4 and 5, respectively.

V. CONCLUSIONS

We have exhibited a filtered backprojection reconstruction formula for SAR imaging from arbitrary (known) flight paths and non-flat (known) earth topography, in the presence of noise and clutter. We have shown that under the assumption of stationarity of the statistics of the target, clutter, and noise, the filter in the backprojection algorithm should be chosen as (33). This filter automatically gives less weight to those frequencies at which the noise and clutter have significant energy.

Since the amplitude A involves the power spectral density of the waveform, the form (33) provides information on how the waveform p should be chosen. Exploration of this leads to the waveform (40) and the filter (41). Numerical simulations presented in

The approach outlined in this paper, in which the backprojection phase is assumed known, is most useful for problems in which the phase itself is subject to only minimal uncertainty and it is the noise and clutter that are limiting features. For such problems, making use of accurate phase information allows us to avoid smoothing in the image; moreover, the visible singularities appear in the correct locations and orientations.

ACKNOWLEDGMENTS

We are grateful to the Air Force Office of Scientific Research¹ for supporting this work under agreements F49620-03-1-0051 and FA9550-04-1-0223.

REFERENCES

- [1] G. Beylkin and R. Burridge, "Linearized inverse scattering problems in acoustics and elasticity", *Wave Motion* 12 (1990) 15–52.
- [2] G. Beylkin, "Imaging of discontinuities in the inverse scattering problem by inversion of a causal generalized Radon transform", *J. Math. Phys.*, 26 (1985) 99–108.
- [3] N. Bleistein, J. K. Cohen, and J.W. Stockwell, *The Mathematics of Multidimensional Seismic Inversion*, Springer, New York, 2000.
- [4] Mijdat etin and W. Clem Karl, "Superresolution and edge-preserving reconstruction of complex-valued synthetic aperture radar images," *IEEE International Conference on Image Processing*, vol. 1, pp. 701-704, Vancouver, Canada, September 2000.
- [5] Mijdat Cetin, W. Clem Karl, and Alan S. Willsky, "Edge-Preserving Image Reconstruction for Coherent Imaging Applications", *IEEE International Conference on Image Processing*, vol. 2, pp. 481-484, Rochester, New York, September 2002.
- [6] J.C. Curlander and R.N. McDonough, *Synthetic Aperture Radar*, Wiley, New York, 1991.
- [7] W. C. Carrar, R. G. Goodman, R. M. Majewski, *Spotlight Synthetic Aperture Radar: Signal Processing Algorithms*, Artech House, Boston, 1995.
- [8] L.J. Cutrona, "Synthetic Aperture Radar", in *Radar Handbook*, second edition, ed. M. Skolnik, McGraw-Hill, New York, 1990.
- [9] J.J. Duistermaat, *Fourier Integral Operators*, Birkhauser, Boston, 1996.
- [10] C. Elachi, *Spaceborne Radar Remote Sensing: Applications and Techniques*, IEEE Press, New York, 1987.
- [11] J.A. Fawcett, "Inversion of N-dimensional spherical means, *SIAM J. Appl. Math.* 45 (1985) 336–341.
- [12] G. Franceschetti and R. Lanari, *Synthetic Aperture Radar Processing*, CRC Press, New York, 1999.
- [13] A. Grigis and J. Sjöstrand, *Microlocal Analysis for Differential Operators: An Introduction*, London Mathematical Society Lecture Note Series vol. 196, Cambridge University Press, 1994.
- [14] H. Hellsten and L.E. Andersson, "An inverse method for the processing of synthetic aperture radar data", *Inverse Problems* 3 (1987), 111–124.
- [15] G.T. Herman, H.K. Tuy, K.J. Langenberg and P.C. Sabatier *Basic Methods of Tomography and Inverse Problems*, Adam Hilger, Philadelphia, PA, 1988.
- [16] K.J. Langenberg, M. Brandfass, K. Mayer, T. Kreutter, A. Brüll, P. Felinger, D. Huo, "Principles of microwave imaging and inverse scattering", *EARSeL Advances in Remote Sensing*, 2 (1993) 163–186.
- [17] A. Louis and E.T. Quinto, "Local Tomographic Methods in SONAR", in *Surveys on Solution Methods for Inverse Problems*, Ed. D. Colton, H. W. Engl, A.K. Louis, J.R. McLaughlin and W. Rundell, Springer Verlag, New York, 2000.
- [18] S. Nilsson, "Application of fast backprojection techniques for some inverse problems of integral geometry", *Linköping Studies in Science and Technology*, Dissertation No. 499 (1997).
- [19] C.J. Nolan and M. Cheney, "Synthetic Aperture Inversion for Arbitrary Flight Paths and Non-Flat Topography", *IEEE Transactions on Image Processing* 12 (Sept. 2003) 1035-1043.
- [20] C. J. Nolan and W. W. Symes, "Global solution of a linearized inverse problem for the acoustic wave equation", *Comm. in P.D.E.*, Vol. 22, Nos 5-6, 1997.
- [21] E.T. Quinto, "Singularities of the X-ray transform and limited data tomography in R^2 and R^3 ", *SIAM J. Math. Anal.*, 24(1993), 1215-1225.

¹Consequently the U.S. Government is authorized to reproduce and distribute reprints for Governmental purposes notwithstanding any copyright notation thereon. The views and conclusions contained herein are those of the authors and should not be interpreted as necessarily representing the official policies or endorsements, either expressed or implied, of the Air Force Research Laboratory or the U.S. Government.

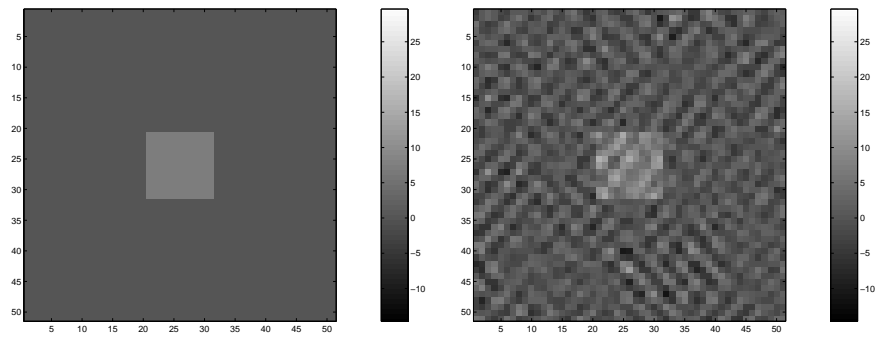


Fig. 2. (Left) Target, and (Right) target embedded in clutter when $SCR = -12\text{dB}$.

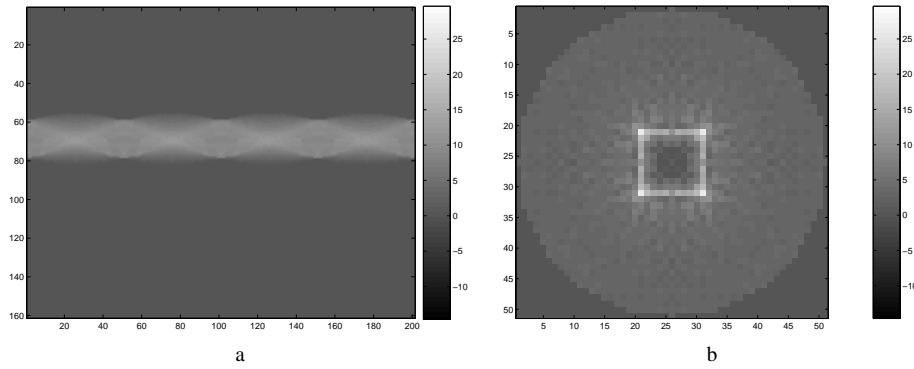


Fig. 3. (Left) Projection data of the target and (Right) its reconstruction.

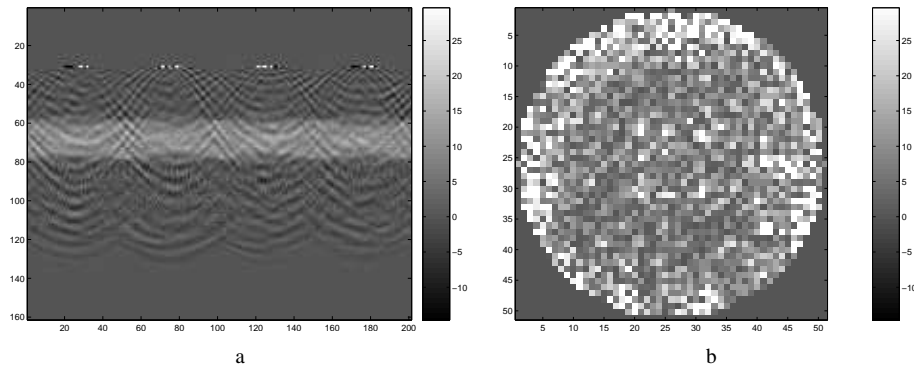


Fig. 4. (Left) Projection data of target embedded in clutter with $SCR = -12\text{dB}$ when $P = 1$, and (Right) its reconstruction.

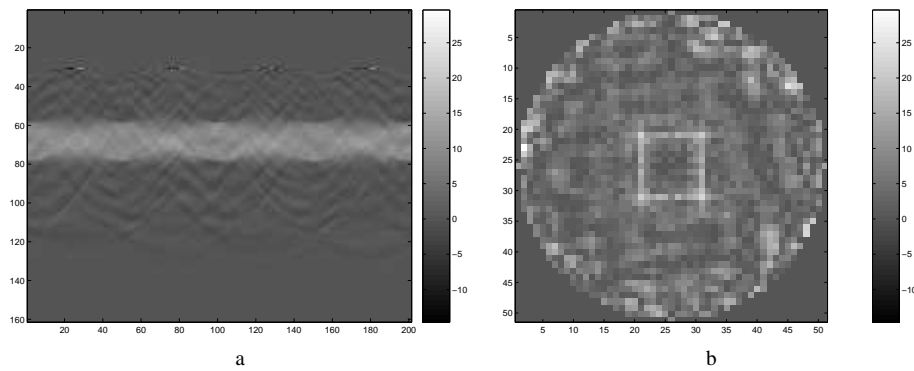


Fig. 5. (Left) Projection data target embedded in clutter when $SCR = -12\text{dB}$ when P is chosen as in (40), and (Right) its reconstruction.

- [23] M. Soumekh, D. Nobels, M. Wicks, and G. Genello, "Signal processing of wide-bandwidth and wide-beamwidth P-3 SAR data", IEEE Trans. on Aerospace and Electronic Systems 37 (2001) 1122-1141.
- [24] F. Trèves, Basic Linear Partial Differential Equations, Academic Press, New York, 1975.
- [25] F. Trèves, Introduction to Pseudodifferential and Fourier Integral Operators, volumes I and II, Plenum Press, New York, 1980.
- [26] L.M.H. Ulander and P.-O. Frölund, "Ultra-wideband SAR interferometry", IEEE Trans. on Geoscience and Remote Sensing, vol. 36 no. 5, September 1998, 1540–1550.
- [27] L.M.H. Ulander and H. Hellsten, "Low-frequency ultra-wideband array-antenna SAR for stationary and moving target imaging", conference proceedings for the SPIE 13th Annual International Symposium on Aerosense, Orlando, Florida, April 1999.
- [28] B. Yazici and M. Cheney "Synthetic aperture inversion for arbitrary flight paths in the presence of noise and clutter", IEEE International Radar Conference, Arlington, Virginia, May 2005.